Study of decay dynamics and *CP* asymmetry in $D^+ \to K_L^0 e^+ \nu_e$ decay

M. Ablikim,[1] M. N. Achasov,[9,f] X. C. Ai,[1] O. Albayrak,[5] M. Albrecht,[4] D. J. Ambrose,[44] A. Amoroso,[49a,49c] F. F. An,[1] Q. An,[46,a] J. Z. Bai,[1] R. Baldini Ferroli,[20a] Y. Ban,[31] D. W. Bennett,[19] J. V. Bennett,[5] M. Bertani,[20a] D. Bettoni,[21a] J. M. Bian,[43] F. Bianchi,[49a,49c] E. Boger,[23,d] I. Boyko,[23] R. A. Briere,[5] H. Cai,[51] X. Cai,[1,a] O. Cakir,[40a,b] A. Calcaterra,[20a] G. F. Cao,[1] S. A. Cetin,[40b] J. F. Chang,[1,a] G. Chelkov,[23,d,e] G. Chen,[1] H. S. Chen,[1] H. Y. Chen,[2] J. C. Chen,[1] M. L. Chen,[1,a] S. Chen,[41] S. J. Chen,[29] X. Chen,[1,a] X. R. Chen,[26] Y. B. Chen,[1,a] H. P. Cheng,[17] X. K. Chu,[31] G. Cibinetto,[21a] H. L. Dai,[1,a] J. P. Dai,[34] A. Dbeyssi,[14] D. Dedovich,[23] Z. Y. Deng,[1] A. Denig,[22] I. Denysenko,[23] M. Destefanis,[49a,49c] F. De Mori,[49a,49c] Y. Ding,[27] C. Dong,[30] J. Dong,[1,a] L. Y. Dong,[1] M. Y. Dong,[1,a] S. X. Du,[53] P. F. Duan,[1] J. Z. Fan,[39] J. Fang,[1,a] S. S. Fang,[1] X. Fang,[46,a] Y. Fang,[1] L. Fava,[49a,49c] F. Feldbauer,[22] G. Felici,[20a] C. Q. Feng,[46,a] E. Fioravanti,[21a] M. Fritsch,[14,22] C. D. Fu,[1] Q. Gao,[1] X. L. Gao,[46,a] X. Y. Gao,[2] Y. Gao,[39] Z. Gao,[46,a] I. Garzia,[21a] K. Goetzen,[10] W. X. Gong,[1,a] W. Gradl,[22] M. Greco,[49a,49c] M. H. Gu,[1,a] Y. T. Gu,[12] Y. H. Guan,[1] A. Q. Guo,[1] L. B. Guo,[28] R. P. Guo,[1] Y. Guo,[1] Y. P. Guo,[22] Z. Haddadi,[25] A. Hafner,[22] S. Han,[51] X. Q. Hao,[15] F. A. Harris,[42] K. L. He,[1] T. Held,[4] Y. K. Heng,[1,a] Z. L. Hou,[1] C. Hu,[28] H. M. Hu,[1] J. F. Hu,[49a,49c] T. Hu,[1,a] Y. Hu,[1] G. M. Huang,[6] G. S. Huang,[46,a] J. S. Huang,[15] X. T. Huang,[33] Y. Huang,[29] T. Hussain,[48] Q. Ji,[1] Q. P. Ji,[30] X. B. Ji,[1] X. L. Ji,[1,a] L. W. Jiang,[51] X. S. Jiang,[1,a] X. Y. Jiang,[30] J. B. Jiao,[33] Z. Jiao,[17] D. P. Jin,[1,a] S. Jin,[1] T. Johansson,[50] A. Julin,[43] N. Kalantar-Nayestanaki,[25] X. L. Kang,[1] X. S. Kang,[30] M. Kavatsyuk,[25] B. C. Ke,[5] P. Kiese,[22] R. Kliemt,[14] B. Kloss,[22] O. B. Kolcu,[40b,i] B. Kopf,[4] M. Kornicer,[42] W. Kuehn,[24] A. Kupsc,[50] J. S. Lange,[24] M. Lara,[19] P. Larin,[14] C. Leng,[49c] C. Li,[50] Cheng Li,[46,a] D. M. Li,[53] F. Li,[1,a] F. Y. Li,[31] G. Li,[1] H. B. Li,[1] H. J. Li,[1] J. C. Li,[1] Jin Li,[32] K. Li,[33] K. Li,[13] Lei Li,[3] P. R. Li,[41] T. Li,[33] W. D. Li,[1] W. G. Li,[1] X. L. Li,[33] X. M. Li,[12] X. N. Li,[1,a] X. Q. Li,[30] Z. B. Li,[38] H. Liang,[46,a] J. J. Liang,[12] Y. F. Liang,[36] Y. T. Liang,[24] G. R. Liao,[11] D. X. Lin,[14] B. J. Liu,[1] C. X. Liu,[1] D. Liu,[46,a] F. H. Liu,[35] Fang Liu,[1] Feng Liu,[6] H. B. Liu,[12] H. H. Liu,[1] H. H. Liu,[16] H. M. Liu,[1] J. Liu,[1] J. B. Liu,[46,a] J. P. Liu,[51] J. Y. Liu,[1] K. Liu,[39] K. Y. Liu,[27] L. D. Liu,[31] P. L. Liu,[1,a] Q. Liu,[41] S. B. Liu,[46,a] X. Liu,[26] Y. B. Liu,[30] Z. A. Liu,[1,a] Zhiqing Liu,[22] H. Loehner,[25] X. C. Lou,[1,a,h] H. J. Lu,[17] J. G. Lu,[1,a] Y. Lu,[1] Y. P. Lu,[1,a] C. L. Luo,[28] M. X. Luo,[52] T. Luo,[42] X. L. Luo,[1,a] X. R. Lyu,[41] F. C. Ma,[27] H. L. Ma,[1] L. L. Ma,[33] M. M. Ma,[1] Q. M. Ma,[1] T. Ma,[1] X. N. Ma,[30] X. Y. Ma,[1,a] F. E. Maas,[14] M. Maggiora,[49a,49c] Y. J. Mao,[31] Z. P. Mao,[1] S. Marcello,[49a,49c] J. G. Messchendorp,[25] J. Min,[1,a] R. E. Mitchell,[19] X. H. Mo,[1,a] Y. J. Mo,[6] C. Morales Morales,[14] K. Moriya,[19] N. Yu. Muchnoi,[9,f] H. Muramatsu,[43] Y. Nefedov,[23] F. Nerling,[14] I. B. Nikolaev,[9,f] Z. Ning,[1,a] S. Nisar,[8] S. L. Niu,[1,a] X. Y. Niu,[1] S. L. Olsen,[32] Q. Ouyang,[1,a] S. Pacetti,[20b] Y. Pan,[46,a] P. Patteri,[20a] M. Pelizaeus,[4] H. P. Peng,[46,a] K. Peters,[10] J. Pettersson,[50] J. L. Ping,[28] R. G. Ping,[1] R. Poling,[43] V. Prasad,[1] M. Qi,[29] S. Qian,[1,a] C. F. Qiao,[41] L. Q. Qin,[33] N. Qin,[51] X. S. Qin,[1] Z. H. Qin,[1,a] J. F. Qiu,[1] K. H. Rashid,[48] C. F. Redmer,[22] M. Ripka,[22] G. Rong,[1] Ch. Rosner,[14] X. D. Ruan,[12] A. Sarantsev,[23,g] M. Savrié,[21b] K. Schoenning,[50] S. Schumann,[22] W. Shan,[31] M. Shao,[46,a] C. P. Shen,[2] P. X. Shen,[30] X. Y. Shen,[1] H. Y. Sheng,[1] M. Shi,[1] W. M. Song,[1] X. Y. Song,[1] S. Sosio,[49a,49c] S. Spataro,[49a,49c] G. X. Sun,[1] J. F. Sun,[15] S. S. Sun,[1] X. H. Sun,[1] Y. J. Sun,[46,a] Y. Z. Sun,[1] Z. J. Sun,[1,a] Z. T. Sun,[19] C. J. Tang,[36] X. Tang,[1] I. Tapan,[40c] E. H. Thorndike,[44] M. Tiemens,[25] M. Ullrich,[24] I. Uman,[40b] G. S. Varner,[42] B. Wang,[30] D. Wang,[31] D. Y. Wang,[31] K. Wang,[1,a] L. L. Wang,[1] L. S. Wang,[1] M. Wang,[33] P. Wang,[1] P. L. Wang,[1] S. G. Wang,[31] W. Wang,[1,a] W. P. Wang,[46,a] X. F. Wang,[39] Y. D. Wang,[14] Y. F. Wang,[1,a] Y. Q. Wang,[22] Z. Wang,[1,a] Z. G. Wang,[1,a] Z. H. Wang,[46,a] Z. Y. Wang,[1] Z. Y. Wang,[1] T. Weber,[22] D. H. Wei,[11] J. B. Wei,[31] P. Weidenkaff,[22] S. P. Wen,[1] U. Wiedner,[4] M. Wolke,[50] L. H. Wu,[1] L. J. Wu,[1] Z. Wu,[1,a] L. Xia,[46,a] L. G. Xia,[39] Y. Xia,[18] D. Xiao,[1] H. Xiao,[47] Z. J. Xiao,[28] Y. G. Xie,[1,a] Q. L. Xiu,[1,a] G. F. Xu,[1] J. J. Xu,[1] L. Xu,[1] Q. J. Xu,[13] X. P. Xu,[37] L. Yan,[49a,49c] W. B. Yan,[46,a] W. C. Yan,[46,a] Y. H. Yan,[18] H. J. Yang,[34] H. X. Yang,[1] L. Yang,[51] Y. Yang,[6] Y. X. Yang,[11] M. Ye,[1,a] M. H. Ye,[7] J. H. Yin,[1] B. X. Yu,[1,a] C. X. Yu,[30] J. S. Yu,[26] C. Z. Yuan,[1] W. L. Yuan,[29] Y. Yuan,[1] A. Yuncu,[40b,b] A. A. Zafar,[48] A. Zallo,[20a] Y. Zeng,[18] Z. Zeng,[46,a] B. X. Zhang,[1] B. Y. Zhang,[1,a] C. Zhang,[29] C. C. Zhang,[1] D. H. Zhang,[1] H. H. Zhang,[38] H. Y. Zhang,[1,a] J. Zhang,[1] J. J. Zhang,[1] J. L. Zhang,[1] J. Q. Zhang,[1] J. W. Zhang,[1,a] J. Y. Zhang,[1] J. Z. Zhang,[1] K. Zhang,[1] L. Zhang,[1] X. Y. Zhang,[33] Y. Zhang,[1] Y. N. Zhang,[41] Y. H. Zhang,[1,a] Y. T. Zhang,[46,a] Yu Zhang,[41] Z. H. Zhang,[6] Z. P. Zhang,[46] Z. Y. Zhang,[51] G. Zhao,[1] J. W. Zhao,[1,a] J. Y. Zhao,[1] J. Z. Zhao,[1,a] Lei Zhao,[46,a] Ling Zhao,[1] M. G. Zhao,[30] Q. Zhao,[1] Q. W. Zhao,[1] S. J. Zhao,[53] T. C. Zhao,[1] Y. B. Zhao,[1,a] Z. G. Zhao,[46,a] A. Zhemchugov,[23,d] B. Zheng,[47] J. P. Zheng,[1,a] W. J. Zheng,[33] Y. H. Zheng,[41] B. Zhong,[28] L. Zhou,[1,a] X. Zhou,[51] X. K. Zhou,[46,a] X. R. Zhou,[46,a] X. Y. Zhou,[1] K. Zhu,[1] K. J. Zhu,[1,a] S. Zhu,[1] S. H. Zhu,[45] X. L. Zhu,[39] Y. C. Zhu,[46,a] Y. S. Zhu,[1] Z. A. Zhu,[1] J. Zhuang,[1,a] L. Zotti,[49a,49c] B. S. Zou,[1] and J. H. Zou[1]

(BESIII Collaboration)

[1]*Institute of High Energy Physics, Beijing 100049, People's Republic of China*
[2]*Beihang University, Beijing 100191, People's Republic of China*
[3]*Beijing Institute of Petrochemical Technology, Beijing 102617, People's Republic of China*

[4]*Bochum Ruhr-University, D-44780 Bochum, Germany*
[5]*Carnegie Mellon University, Pittsburgh, Pennsylvania 15213, USA*
[6]*Central China Normal University, Wuhan 430079, People's Republic of China*
[7]*China Center of Advanced Science and Technology, Beijing 100190, People's Republic of China*
[8]*COMSATS Institute of Information Technology, Lahore, Defence Road, Off Raiwind Road, 54000 Lahore, Pakistan*
[9]*G.I. Budker Institute of Nuclear Physics SB RAS (BINP), Novosibirsk 630090, Russia*
[10]*GSI Helmholtzcentre for Heavy Ion Research GmbH, D-64291 Darmstadt, Germany*
[11]*Guangxi Normal University, Guilin 541004, People's Republic of China*
[12]*GuangXi University, Nanning 530004, People's Republic of China*
[13]*Hangzhou Normal University, Hangzhou 310036, People's Republic of China*
[14]*Helmholtz Institute Mainz, Johann-Joachim-Becher-Weg 45, D-55099 Mainz, Germany*
[15]*Henan Normal University, Xinxiang 453007, People's Republic of China*
[16]*Henan University of Science and Technology, Luoyang 471003, People's Republic of China*
[17]*Huangshan College, Huangshan 245000, People's Republic of China*
[18]*Hunan University, Changsha 410082, People's Republic of China*
[19]*Indiana University, Bloomington, Indiana 47405, USA*
[20a]*INFN Laboratori Nazionali di Frascati, I-00044 Frascati, Italy*
[20b]*INFN and University of Perugia, I-06100 Perugia, Italy*
[21a]*INFN Sezione di Ferrara, I-44122 Ferrara, Italy*
[21b]*University of Ferrara, I-44122 Ferrara, Italy*
[22]*Johannes Gutenberg University of Mainz, Johann-Joachim-Becher-Weg 45, D-55099 Mainz, Germany*
[23]*Joint Institute for Nuclear Research, 141980 Dubna, Moscow region, Russia*
[24]*Justus Liebig University Giessen, II. Physikalisches Institut, Heinrich-Buff-Ring 16, D-35392 Giessen, Germany*
[25]*KVI-CART, University of Groningen, NL-9747 AA Groningen, Netherlands*
[26]*Lanzhou University, Lanzhou 730000, People's Republic of China*
[27]*Liaoning University, Shenyang 110036, People's Republic of China*
[28]*Nanjing Normal University, Nanjing 210023, People's Republic of China*
[29]*Nanjing University, Nanjing 210093, People's Republic of China*
[30]*Nankai University, Tianjin 300071, People's Republic of China*
[31]*Peking University, Beijing 100871, People's Republic of China*
[32]*Seoul National University, Seoul, 151-747 Korea*
[33]*Shandong University, Jinan 250100, People's Republic of China*
[34]*Shanghai Jiao Tong University, Shanghai 200240, People's Republic of China*
[35]*Shanxi University, Taiyuan 030006, People's Republic of China*
[36]*Sichuan University, Chengdu 610064, People's Republic of China*
[37]*Soochow University, Suzhou 215006, People's Republic of China*
[38]*Sun Yat-Sen University, Guangzhou 510275, People's Republic of China*
[39]*Tsinghua University, Beijing 100084, People's Republic of China*
[40a]*Istanbul Aydin University, 34295 Sefakoy, Istanbul, Turkey*
[40b]*Istanbul Bilgi University, 34060 Eyup, Istanbul, Turkey*
[40c]*Uludag University, 16059 Bursa, Turkey*
[41]*University of Chinese Academy of Sciences, Beijing 100049, People's Republic of China*
[42]*University of Hawaii, Honolulu, Hawaii 96822, USA*
[43]*University of Minnesota, Minneapolis, Minnesota 55455, USA*
[44]*University of Rochester, Rochester, New York 14627, USA*
[45]*University of Science and Technology Liaoning, Anshan 114051, People's Republic of China*
[46]*University of Science and Technology of China, Hefei 230026, People's Republic of China*
[47]*University of South China, Hengyang 421001, People's Republic of China*
[48]*University of the Punjab, Lahore-54590, Pakistan*
[49a]*University of Turin, I-10125 Turin, Italy*
[49b]*University of Eastern Piedmont, I-15121 Alessandria, Italy*
[49c]*INFN, I-10125 Turin, Italy*
[50]*Uppsala University, Box 516, SE-75120 Uppsala, Sweden*
[51]*Wuhan University, Wuhan 430072, People's Republic of China*

[52]*Zhejiang University, Hangzhou 310027, People's Republic of China*
[53]*Zhengzhou University, Zhengzhou 450001, People's Republic of China*
(Received 2 October 2015; published 29 December 2015)

Using 2.92 fb^{-1} of electron-positron annihilation data collected at $\sqrt{s} = 3.773$ GeV with the BESIII detector, we obtain the first measurements of the absolute branching fraction $\mathcal{B}(D^+ \to K_L^0 e^+ \nu_e) = (4.481 \pm 0.027(\text{stat}) \pm 0.103(\text{sys}))\%$ and the *CP* asymmetry $A_{CP}^{D^+ \to K_L^0 e^+ \nu_e} = (-0.59 \pm 0.60(\text{stat}) \pm 1.48(\text{sys}))\%$. From the $D^+ \to K_L^0 e^+ \nu_e$ differential decay rate distribution, the product of the hadronic form factor and the magnitude of the Cabibbo-Kobayashi-Maskawa matrix element, $f_+^K(0)|V_{cs}|$, is determined to be $0.728 \pm 0.006(\text{stat}) \pm 0.011(\text{sys})$. Using $|V_{cs}|$ from the SM constrained fit with the measured $f_+^K(0)|V_{cs}|$, $f_+^K(0) = 0.748 \pm 0.007(\text{stat}) \pm 0.012(\text{sys})$ is obtained, and utilizing the unquenched Lattice QCD (LQCD) calculation for $f_+^K(0)$, $|V_{cs}| = 0.975 \pm 0.008(\text{stat}) \pm 0.015(\text{sys}) \pm 0.025(\text{LQCD})$.

DOI: 10.1103/PhysRevD.92.112008 PACS numbers: 13.20.Fc, 11.30.Er, 12.15.Hh

I. INTRODUCTION

In the Standard Model (SM), violation of the combined charge-conjugation and parity symmetries (*CP*) arises from a nonvanishing irreducible phase in the Cabibbo-Kobayashi-Maskawa (CKM) flavor-mixing matrix [1,2]. Although, in the SM, *CP* violation in the charm sector is expected to be very small, $\mathcal{O}(10^{-3})$ or below [3], Ref. [4] finds that $K^0 - \bar{K}^0$ mixing will give rise to a clean *CP* violation signal of a magnitude of $-2\text{Re}(\epsilon) \approx -3.3 \times 10^{-3}$ in the semileptonic decays $D^+ \to K_L^0(K_S^0)e^+\nu_e$.

Semileptonic decays of mesons allow the determination of various important SM parameters, including elements of the CKM matrix, which in turn allows the physics of the SM to be tested at its most fundamental level. In the limit of zero electron mass, the differential decay rate for a D semileptonic decay with a pseudoscalar meson P is given by

$$\frac{d\Gamma(D \to Pe\nu_e)}{dq^2} = \frac{G_F^2 |V_{cs(d)}|^2}{24\pi^3} p^3 |f_+(q^2)|^2, \qquad (1)$$

where G_F is the Fermi constant, $V_{cs(d)}$ is the relevant CKM matrix element, p is the momentum of the daughter meson in the rest frame of the parent D, $f_+(q^2)$ is the form factor, and q^2 is the invariant mass squared of the lepton-neutrino system.

In this paper, the first measurements of the absolute branching fraction and the *CP* asymmetry for the decay $D^+ \to K_L^0 e^+ \nu_e$ as well as the form-factor parameters for three different theoretical models that describe the weak hadronic charged currents in $D^+ \to K_L^0 e^+ \nu_e$ are presented. The paper is organized as follows. The BESIII detector and data sample are described in Sec. II. The analysis technique is introduced in Sec. III. In Secs. IV and V, the measurements of the absolute branching fraction, the *CP* asymmetry, and the form-factor parameters for the decay $D^+ \to K_L^0 e^+ \nu_e$ are described. Finally, a summary is provided in Sec. VI.

II. BESIII DETECTOR AND DATA SAMPLE

The analysis presented in this paper is based on a data sample with an integrated luminosity of 2.92 fb^{-1} [5] collected with the BESIII detector [6] at the center-of-mass energy of $\sqrt{s} = 3.773$ GeV. The BESIII detector is a general-purpose detector at the BEPCII [7] double storage rings. The detector has a geometrical acceptance of 93% of the full solid angle. We briefly describe the components of BESIII from the interaction point (IP) outward. A small-cell multilayer drift chamber (MDC), using a helium-based gas to measure momenta and specific ionization of charged particles, is surrounded by a time-of-flight (TOF) system based on plastic scintillators which determines the time of flight of charged particles. A CsI(Tl) electromagnetic calorimeter (EMC) detects electromagnetic showers. These components are all situated inside a superconducting solenoid magnet, which provides a 1.0 T magnetic field parallel to the beam direction. Finally, a multilayer resistive plate counter system installed in the iron flux return yoke of the magnet is used to track muons. The momentum resolution for charged tracks in the MDC is 0.5% for a transverse momentum of 1 GeV/c. The energy resolution

[a]Also at State Key Laboratory of Particle Detection and Electronics, Beijing 100049, Hefei 230026, People's Republic of China.
[b]Also at Ankara University,06100 Tandogan, Ankara, Turkey.
[c]Also at Bogazici University, 34342 Istanbul, Turkey.
[d]Also at the Moscow Institute of Physics and Technology, Moscow 141700, Russia.
[e]Also at the Functional Electronics Laboratory, Tomsk State University, Tomsk 634050, Russia.
[f]Also at the Novosibirsk State University, Novosibirsk 630090, Russia.
[g]Also at the NRC "Kurchatov Institute", Petersburg Nuclear Physics Institute 188300, Gatchina, Russia.
[h]Also at University of Texas at Dallas, Richardson, Texas 75083, USA.
[i]Also at Istanbul Arel University, 34295 Istanbul, Turkey.

for showers in the EMC is 2.5% for 1 GeV photons. More details on the features and capabilities of BESIII can be found elsewhere [6].

The performance of the BESIII detector is simulated using a GEANT4-based [8] Monte Carlo (MC) program. To develop selection criteria and test the analysis technique, several MC samples are used. For the production of $\psi(3770)$, the KKMC [9] package is used; the beam energy spread and the effects of initial-state radiation (ISR) are included. Final-state radiation of charged tracks is taken into account with the PHOTOS package [10]. $\psi(3770) \to D\bar{D}$ events are generated using EVTGEN [11,12], and each D meson is allowed to decay according to the branching fractions in the Particle Data Group (PDG) [13]. We refer to this as the "generic MC." The equivalent luminosity of the MC samples is about ten times that of the data. A sample of $\psi(3770) \to D\bar{D}$ events, in which the D meson decays to the signal semileptonic mode and the $\bar{D}$ decays to one of the hadronic final states used in the tag reconstruction, is referred to as the "signal MC." In both the generic and signal MC samples, the semileptonic decays are generated using the modified pole parametrization [14] (see Sec. V B).

III. EVENT SELECTION

At the $\psi(3770)$ peak, $D\bar{D}$ pairs are produced. First, we select the single-tag (ST) sample in which a D^- is reconstructed in a hadronic decay mode. From the ST sample, the double-tag (DT) events of $D^+ \to K_L^0 e^+ \nu_e$ are selected. The numbers of the ST and DT events are given by

$$N_{\rm ST} = N_{D^+D^-}\mathcal{B}_{\rm tag}\epsilon_{\rm ST}, N_{\rm DT} = N_{D^+D^-}\mathcal{B}_{\rm tag}\mathcal{B}_{\rm sig}\epsilon_{\rm DT}, \quad (2)$$

where $N_{D^+D^-}$ is the number of D^+D^- pairs produced, $N_{\rm ST}$ and $N_{\rm DT}$ are the numbers of the ST and DT events, $\epsilon_{\rm ST}$ and $\epsilon_{\rm DT}$ are the corresponding efficiencies, and $\mathcal{B}_{\rm tag}$ and $\mathcal{B}_{\rm sig}$ are the branching fractions of the hadronic tag decay and the signal decay. In this analysis, the charge-dependent branching fractions are measured, so there is no factor of 2 in Eq. (2). From Eq. (2), we obtain

$$\mathcal{B}_{\rm sig} = \frac{N_{\rm DT}/\epsilon_{\rm DT}}{N_{\rm ST}/\epsilon_{\rm ST}} = \frac{N_{\rm DT}/\epsilon}{N_{\rm ST}}, \quad (3)$$

where $\epsilon = \epsilon_{\rm DT}/\epsilon_{\rm ST}$ is the efficiency of finding a signal candidate in the presence of a ST D, which is obtained from generic MC simulations.

A. Selection of ST events

Each charged track is required to satisfy $|\cos\theta| < 0.93$, where θ is the polar angle with respect to the beam axis. Charged tracks other than those from the K_S^0 are required to have their points of closest approach to the beamline within 10 cm from the IP along the beam axis and within 1 cm in the plane perpendicular to the beam axis. Particle identification for charged hadrons h ($h = \pi, K$) is accomplished by combining the measured energy loss (dE/dx) in the MDC and the flight time obtained from the TOF to form a likelihood $\mathcal{L}(h)$ for each hadron hypothesis. The $K^\pm$ ($\pi^\pm$) candidates are required to satisfy $\mathcal{L}(K) > \mathcal{L}(\pi)$ [$\mathcal{L}(\pi) > \mathcal{L}(K)$].

The K_S^0 candidates are selected from pairs of oppositely charged tracks which satisfy a vertex-constrained fit to a common vertex. The vertices are required to be within 20 cm of the IP along the beam direction; no constraint in the transverse plane is applied. Particle identification is not required, and the two charged tracks are assumed to be pions. We require $|M_{\pi^+\pi^-} - M_{K_S^0}| < 12$ MeV/c^2, where $M_{K_S^0}$ is the nominal K_S^0 mass [13] and 12 MeV/c^2 is about 3 standard deviations of the observed K_S^0 mass resolution. Lastly, the K_S^0 candidate must have a decay length more than 2 standard deviations of the vertex resolution away from the IP.

Reconstructed EMC showers that are separated from the extrapolated positions of any charged tracks by more than 10° are taken as photon candidates. The energy deposited in the nearby TOF counters is included to improve the reconstruction efficiency and energy resolution. Photon candidates must have a minimum energy of 25 MeV for barrel showers ($|\cos\theta| < 0.80$) and 50 MeV for end cap showers ($0.86 < |\cos\theta| < 0.92$). The shower timing is required to be no later than 700 ns after the reconstructed event start time to suppress electronic noise and energy deposits unrelated to the event.

The π^0 candidates are reconstructed from pairs of photons, and the invariant mass $M_{\gamma\gamma}$ is required to satisfy $0.110 < M_{\gamma\gamma} < 0.155$ GeV/c^2. The invariant mass of two photons is constrained to the nominal π^0 mass [13] by a kinematic fit, and the χ^2 of the kinematic fit is required to be less than 20.

We form $D^\pm$ candidates decaying into final hadronic states of $K^\mp\pi^\pm\pi^\pm$, $K^\mp\pi^\pm\pi^\pm\pi^0$, $K_S^0\pi^\pm\pi^0$, $K_S^0\pi^\pm\pi^\pm\pi^\mp$, $K_S^0\pi^\pm$, and $K^+K^-\pi^\pm$. Two variables are used to identify valid ST D candidates: $\Delta E \equiv E_D - E_{\rm beam}$, the energy difference between the energy of the ST D (E_D) and the beam energy ($E_{\rm beam}$), and the beam-constrained mass $M_{\rm BC} \equiv \sqrt{E_{\rm beam}^2/c^4 - |\vec{p}_D|^2/c^2}$, where $\vec{p}_D$ is the momentum of the D. The ST D signal should peak at the nominal D mass in the $M_{\rm BC}$ distribution and around zero in the ΔE distribution. We only accept one candidate per mode; when multiple candidates are present in an event, the one with the smallest $|\Delta E|$ is kept. Backgrounds are suppressed by the mode-dependent ΔE requirements listed in Table I.

The ST yields of data are determined by binned maximum likelihood fits to the $M_{\rm BC}$ distributions. The signal MC line shape is used to describe the D signal, and an ARGUS [15] function is used to model the combinatorial backgrounds from the continuum light hadron production,

TABLE I. Requirements on ΔE for the ST D candidates. The limits are set at approximately 3 standard deviations of the ΔE resolution.

Mode	Requirement (GeV)
$D^{\pm} \to K^{\mp}\pi^{\pm}\pi^{\pm}$	$-0.030 < \Delta E < 0.030$
$D^{\pm} \to K^{\mp}\pi^{\pm}\pi^{\pm}\pi^{0}$	$-0.052 < \Delta E < 0.039$
$D^{\pm} \to K^{0}_{S}\pi^{\pm}\pi^{0}$	$-0.057 < \Delta E < 0.040$
$D^{\pm} \to K^{0}_{S}\pi^{\pm}\pi^{\pm}\pi^{\mp}$	$-0.034 < \Delta E < 0.034$
$D^{\pm} \to K^{0}_{S}\pi^{\pm}$	$-0.032 < \Delta E < 0.032$
$D^{\pm} \to K^{+}K^{-}\pi^{\pm}$	$-0.030 < \Delta E < 0.030$

$\gamma_{\rm ISR}\psi(3686)$, $\gamma_{\rm ISR}J/\psi$, and nonsignal $D\bar{D}$ decays. A Gaussian function, with the standard deviation and the central value as free parameters, is convoluted with the line shape to account for imperfect modeling of the detector resolution and beam energy.

The charge-conjugated tag modes are fitted simultaneously, with the same signal and ARGUS background shapes for the tag and charge conjugated modes. The numbers of signal and background events are left free. Figures 1 and 2 show the fits to the $M_{\rm BC}$ distributions of the ST D^{+} and D^{-} candidates in data, respectively. The ST yields are obtained by integrating the fitted signal function in the narrower $M_{\rm BC}$ signal region ($1.86 < M_{\rm BC} < 1.88$ GeV/c^2) and are listed in Table II.

B. Selection of DT events

After ST D candidates are identified, we search for electrons and K^{0}_{L} showers among the unused charged tracks and neutral showers. For electron identification, the ratio $\mathcal{R}'_{\mathcal{L}'}(e) \equiv \mathcal{L}'(e)/[\mathcal{L}'(e)+\mathcal{L}'(\pi)+\mathcal{L}'(K)]$ is required to be greater than 0.8, where the likelihood $\mathcal{L}'(i)$ for the hypothesis $i = e$, π or K is formed by combining the EMC information with the dE/dx and TOF information. The energy lost by electrons to bremsstrahlung photons is partially recovered by adding the energy of showers that are within 5° of the electron and are not matched to other charged particles. The selected electron is required to have the opposite charge from the ST D. Events that include charged tracks other than those of the ST D and the electron are vetoed.

Because of the long K^{0}_{L} lifetime, very few K^{0}_{L} decay in the MDC. However, most K^{0}_{L} will interact in the material of the EMC, which gives their position, and deposit part of their energy. We search for K^{0}_{L} candidates by reconstructing all other particles in the event; we then loop over unused reconstructed neutral showers, taking the direction to the shower as the flight direction of the K^{0}_{L}. Using energy-momentum conservation and the constraint $U_{\rm miss} = 0$, we calculate the momentum magnitude $|\vec{p}_{K^{0}_{L}}|$ of the K^{0}_{L} and the four-vector of the unreconstructed neutrino in the event. The variable $U_{\rm miss}$ is expected to peak at zero for semileptonic decay candidates and is defined as

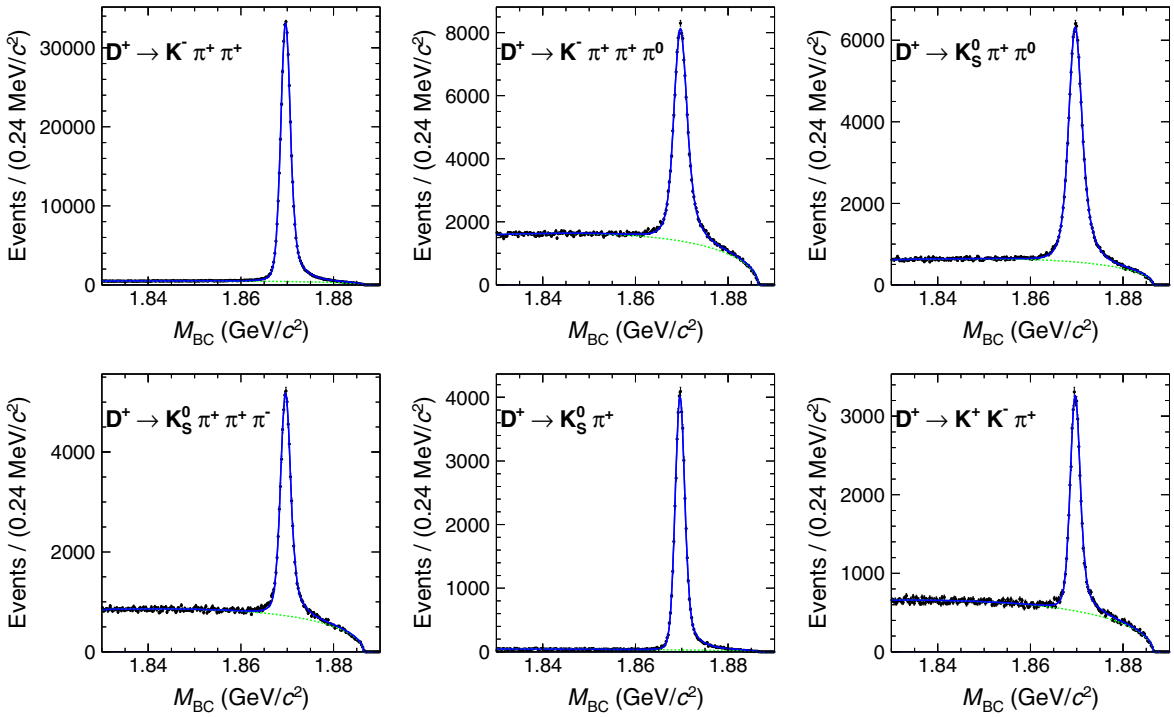

FIG. 1 (color online). Fits to the $M_{\rm BC}$ distributions of the ST D^{+} candidates for data. The dots with error bars are for data, and the blue solid curves are the results of the fits. The green dashed curves are the fitted backgrounds.

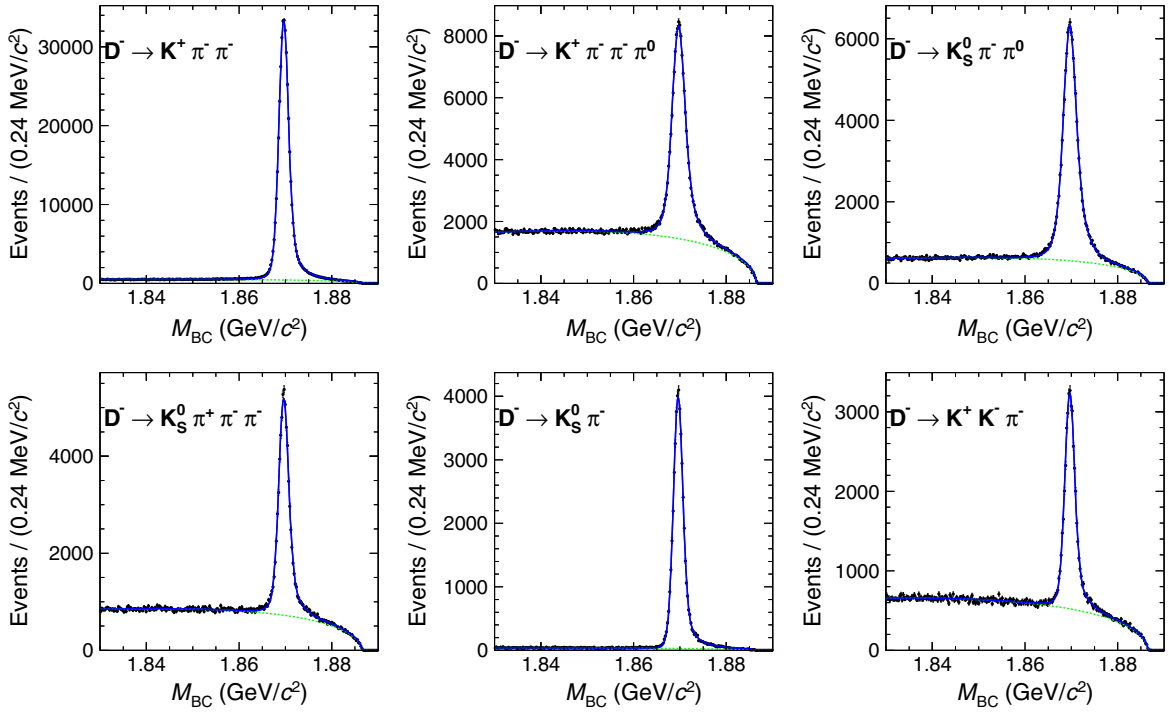

FIG. 2 (color online). Fits to the $M_{\rm BC}$ distributions of the ST D^- candidates for data. The dots with error bars are data, and the blue solid curves are the results of the fits. The green dashed curves are the fitted backgrounds.

TABLE II. Summary of the ST yields ($N_{\rm ST}$), the DT yields ($N_{\rm DT}$), the peaking background rates for the DT candidates ($f_{\rm bkg}^{\rm peak}$), the detection efficiency (ϵ), and the branching fraction for signal decay for each ST mode ($\mathcal{B}_{\rm sig}$). The averages are the weighted average of the individual ST mode branching fractions. The uncertainties are statistical.

		$D^+ \to K_L^0 e^+ \nu_e$			
Tag mode	$N_{\rm ST}$	$N_{\rm DT}$	$f_{\rm bkg}^{\rm peak}(\%)$	$\epsilon(\%)$	$\mathcal{B}_{\rm sig}(\%)$
$D^- \to K^+\pi^-\pi^-$	410200 ± 670	10492 ± 103	41.83 ± 0.28	33.96 ± 0.10	4.381 ± 0.050
$D^- \to K^+\pi^-\pi^-\pi^0$	120060 ± 457	3324 ± 64	44.78 ± 0.49	33.14 ± 0.19	4.613 ± 0.103
$D^- \to K_S^0\pi^-\pi^0$	102136 ± 378	2658 ± 56	38.93 ± 0.58	35.67 ± 0.21	4.456 ± 0.108
$D^- \to K_S^0\pi^-\pi^-\pi^+$	59158 ± 303	1459 ± 41	40.84 ± 0.76	32.51 ± 0.27	4.488 ± 0.145
$D^- \to K_S^0\pi^-$	47921 ± 225	1287 ± 36	38.90 ± 0.88	35.07 ± 0.32	4.679 ± 0.155
$D^- \to K^+K^-\pi^-$	35349 ± 239	905 ± 32	44.64 ± 0.97	30.98 ± 0.35	4.575 ± 0.190
Average					4.454 ± 0.038
		$D^- \to K_L^0 e^- \bar{\nu}_e$			
Tag mode	$N_{\rm ST}$	$N_{\rm DT}$	$f_{\rm bkg}^{\rm peak}(\%)$	$\epsilon(\%)$	$\mathcal{B}_{\rm sig}(\%)$
$D^+ \to K^-\pi^+\pi^+$	407666 ± 668	10354 ± 103	40.44 ± 0.29	34.02 ± 0.11	4.447 ± 0.051
$D^+ \to K^-\pi^+\pi^+\pi^0$	117555 ± 450	3264 ± 63	42.28 ± 0.52	33.19 ± 0.19	4.829 ± 0.107
$D^+ \to K_S^0\pi^+\pi^0$	101824 ± 378	2642 ± 55	39.06 ± 0.58	35.92 ± 0.21	4.402 ± 0.104
$D^+ \to K_S^0\pi^+\pi^+\pi^-$	59046 ± 303	1533 ± 42	39.68 ± 0.77	33.44 ± 0.27	4.683 ± 0.147
$D^+ \to K_S^0\pi^+$	48240 ± 226	1217 ± 35	38.50 ± 0.88	35.20 ± 0.32	4.408 ± 0.147
$D^+ \to K^+K^-\pi^+$	35742 ± 240	942 ± 32	44.04 ± 0.95	32.40 ± 0.36	4.552 ± 0.181
Average					4.507 ± 0.038

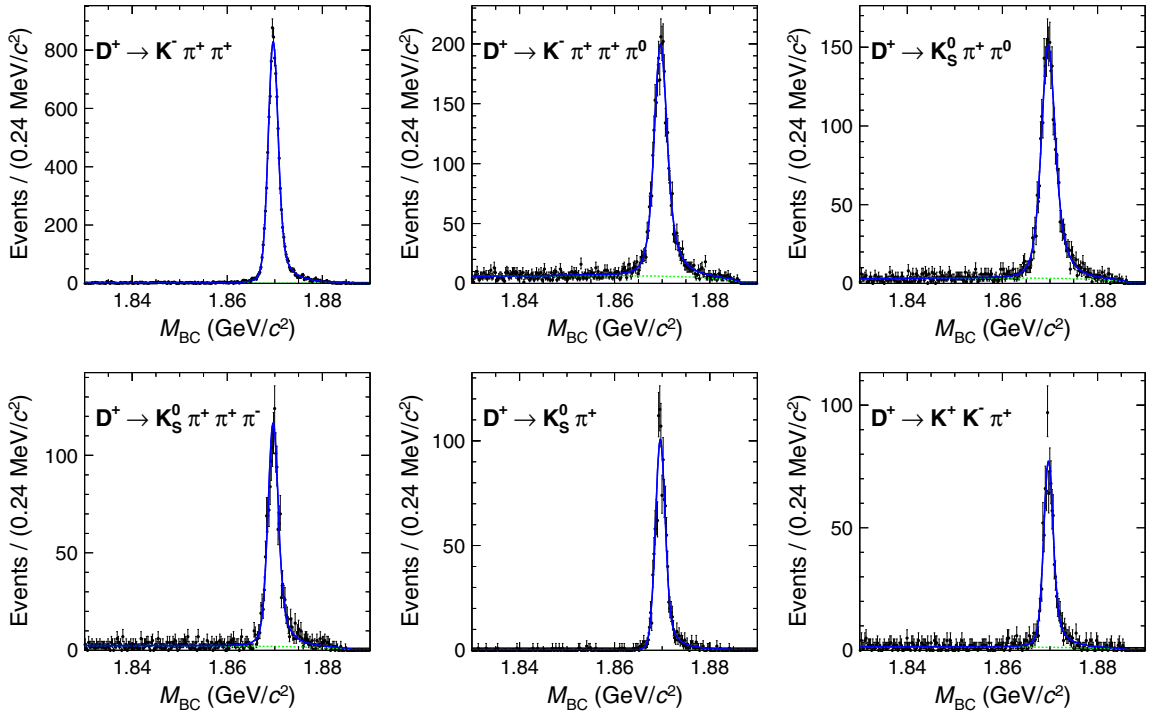

FIG. 3 (color online). Fits to the $M_{\rm BC}$ distributions of the DT D^+ candidates for data. The dots with error bars are for data, and the blue solid curves are the results of the fits. The green dashed curves are the fitted combinatorial backgrounds.

$$U_{\rm miss} \equiv E_{\rm miss} - c|\vec{p}_{\rm miss}|, \tag{4}$$

where

$$\begin{aligned} E_{\rm miss} &= E_{\rm tot} - E_{\rm tag} - E_{K^0_L} - E_e, \\ \vec{p}_{\rm miss} &= \vec{p}_{\rm tot} - \vec{p}_{\rm tag} - \vec{p}_{K^0_L} - \vec{p}_e; \end{aligned} \tag{5}$$

$E_{\rm tot}$, $E_{\rm tag}$, $E_{K^0_L}$, and E_e are the energies of the e^+e^-, the ST D, the K^0_L, and the electron; $\vec{p}_{\rm tot}$, $\vec{p}_{\rm tag}$, $\vec{p}_{K^0_L}$, and $\vec{p}_e$ refer to their momenta. $E_{K^0_L}$ is calculated by $E_{K^0_L} = \sqrt{|\vec{p}_{K^0_L}|^2 + m^2_{K^0_L}}$. In order to suppress background from fake photons, the energy of the K^0_L shower should be greater than 0.1 GeV. We also reject photons that may come from π^0's by rejecting γ in any $\gamma\gamma$ combination with $0.110 < M_{\gamma\gamma} < 0.155$ GeV/c^2. In events with multiple K^0_L shower candidates, the most energetic shower is chosen. The inferred four-momentum of the K^0_L is used to determine the reconstructed q^2, the invariant mass squared of the $e^+\nu_e$ pair, by

$$q^2 = \frac{1}{c^4}(E_{\rm tot} - E_{\rm tag} - E_{K^0_L})^2 - \frac{1}{c^2}|\vec{p}_{\rm tot} - \vec{p}_{\rm tag} - \vec{p}_{K^0_L}|^2. \tag{6}$$

Similar to the determination of the ST yields, we obtain the DT yields of data from the fits to the $M_{\rm BC}$ distributions of the corresponding ST D candidates. Figures 3 and 4 show the fits to the $M_{\rm BC}$ distributions of the DT D^+ and D^- candidates in data, respectively. From the fits, we obtain the DT yields in the data, which are listed in the third column of Table II.

C. Estimation of backgrounds

The K^0_L reconstruction efficiencies of data and MC differ, so the K^0_L reconstruction efficiency of the generic MC is corrected to that of data. The correction factors of K^0_L reconstruction efficiencies are determined from two control samples ($J/\psi \to K^*(892)^\pm K^\mp$ with $K^*(892)^\pm \to K^0_L\pi^\pm$ and $J/\psi \to \phi K^0_L K^\pm\pi^\mp$), which are described in the Appendix. The corrected generic MC samples are used to determine the amount of peaking background and the efficiency for $D^+ \to K^0_L e^+\nu_e$.

We examine the topologies of the corrected generic MC samples to study the composition of the DT samples. In the $M_{\rm BC}$ signal region, the DT D candidates can be divided into the following categories:

(1) Signal: Tag side and signal side correctly matched.
(2) Background:
   (a) Tag-side mismatched events (Bkg I).
   (b) Tag-side matched but signal-side mismatched signal events (Bkg II).
   (c) Tag-side matched but $D \to Xe\nu_e$ no-signal events on the signal side (Bkg III).
   (d) Tag-side matched but $D \to X\mu\nu_\mu$ events on the signal side (Bkg IV).

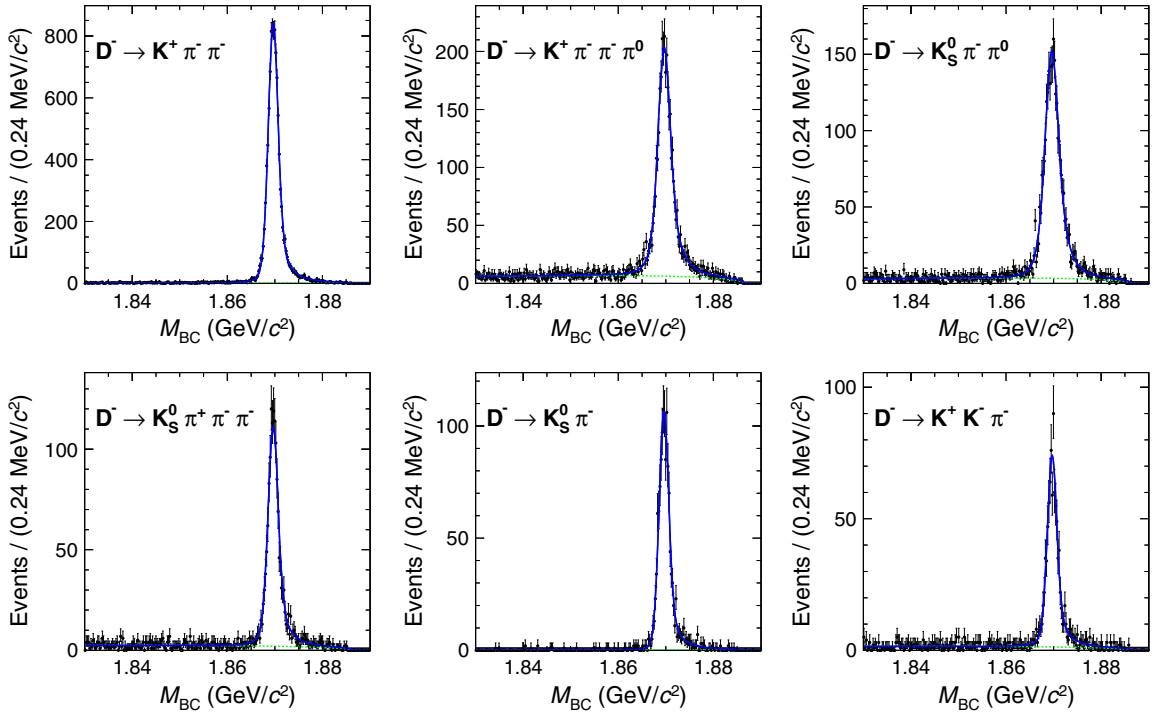

FIG. 4 (color online). Fits to the $M_{\rm BC}$ distributions of the DT D^- candidates for data. The dots with error bars are for data, and the blue solid curves are the results of the fits. The green dashed curves are the fitted combinatorial backgrounds.

(e) Tag-side matched but nonleptonic D decay events on the signal side (Bkg V).

In the selected DT candidates, the proportion of signal events varies from 49% to 58% according to the specific hadronic tag mode. Bkg I comes from $D\bar{D}$ decays in which the hadronic tag D is misreconstructed and non-$D\bar{D}$ processes and varies from 1% to 12% according to the specific hadronic tag mode. Bkg II (∼10%) consists of $D^+ \to K^0_L e^+\nu_e$ events of which the K^0_L shower is misreconstructed. The dominant background in the DT sample is Bkg III (∼24%), which is from $D^+ \to \bar{K}^*(892)^0 e^+\nu_e$ (41.9%), $D^+ \to K^0_S e^+\nu_e$ (41.2%), $D^+ \to \pi^0 e^+\nu_e$ (10.2%), $D^+ \to \eta e^+\nu_e$ (6.0%), and $D^+ \to \omega e^+\nu_e$ (0.7%). Bkg IV (∼3%) consists of $D^+ \to K^0_L \mu^+\nu_\mu$ (65.2%), $D^+ \to \bar{K}^*(892)^0\mu^+\nu_\mu$ (23.3%), and $D^+ \to K^0_S\mu^+\nu_\mu$ (11.5%). Bkg V (∼3%) consists of $D^+ \to \bar{K}^0\pi^+\pi^0$ (78%) and $D^+ \to \bar{K}^0 K^*(892)^+$ (22%).

IV. BRANCHING FRACTION AND *CP* ASYMMETRY

The branching fraction for $D^+ \to K^0_L e^+\nu_e$ ($\mathcal{B}_{\rm sig}$) is determined by

$$\mathcal{B}_{\rm sig} = \frac{N_{\rm DT}(1 - f^{\rm peak}_{\rm bkg})}{\epsilon N_{\rm ST}}, \tag{7}$$

where $N_{\rm DT}$, $N_{\rm ST}$ are the DT and ST yields, $f^{\rm peak}_{\rm bkg}$ is the proportion of peaking backgrounds in the DT candidates (from Bkg II to Bkg V), and ϵ is the efficiency for finding $D^+ \to K^0_L e^+\nu_e$ in the presence of ST D. $f^{\rm peak}_{\rm bkg}$ and ϵ are obtained from the K^0_L efficiency corrected generic MC samples. The $D^+ \to K^0_L e^+\nu_e$ branching fractions for different ST modes are listed in Table II. We obtain $\mathcal{B}(D^+ \to K^0_L e^+\nu_e) = (4.454 \pm 0.038 \pm 0.102)\%$ and $\mathcal{B}(D^- \to K^0_L e^-\bar{\nu}_e) = (4.507 \pm 0.038 \pm 0.104)\%$, which are the weighted averages of the six ST modes for D^+ and D^- separately. Combining these branching fractions, we obtain the averaged branching fraction $\bar{\mathcal{B}}(D^+ \to K^0_L e^+\nu_e) = (4.481 \pm 0.027 \pm 0.103)\%$, which agrees well with the measurement of $\mathcal{B}(D^+ \to K^0_S e^+\nu_e)$ of CLEO-c [16]. The CP asymmetry of $D^+ \to K^0_L e^+\nu_e$ is

$$A_{CP} \equiv \frac{\mathcal{B}(D^+ \to K^0_L e^+\nu_e) - \mathcal{B}(D^- \to K^0_L e^-\bar{\nu}_e)}{\mathcal{B}(D^+ \to K^0_L e^+\nu_e) + \mathcal{B}(D^- \to K^0_L e^-\bar{\nu}_e)} = (-0.59 \pm 0.60 \pm 1.48)\%. \tag{8}$$

This result is consistent with the theoretical prediction in Ref. [4] (-3.3×10^{-3}).

Table III summarizes the systematic uncertainties in the measurements of absolute branching fractions and the CP asymmetry of $D^+ \to K^0_L e^+\nu_e$. A brief description of each systematic uncertainty is provided below.

TABLE III. Systematic uncertainties in the measurements of the absolute branching fraction and the *CP* asymmetry of $D^+ \to K_L^0 e^+ \nu_e$.

Source	$D^+ \to K_L^0 e^+ \nu_e(\%)$	$D^- \to K_L^0 e^- \bar{\nu}_e(\%)$
Electron tracking	0.5	0.5
Electron ID	0.1	0.1
K_L^0 efficiency correction	1.2	1.2
Extra χ^2 cut for K_L^0 efficiency correction	0.8	0.8
Peaking backgrounds in DT	1.6	1.6
$M_{\rm BC}$ fit	Negligible	Negligible
Total (branching fraction)	2.3	2.3
Total (*CP* asymmetry)	2.1	2.1

A. Electron (positron) track-finding and identification efficiency

Uncertainties of electron (positron) track-finding and identification (ID) efficiency are obtained by comparing the track-finding and ID efficiencies for the electrons (positrons) from radiative Bhabha processes in the data and MC. Considering both the $\cos\theta$, where θ is the polar angle of the positron, and momentum distributions of the electrons (positrons) of the signal events, we obtain the two-dimensional weighted uncertainty of electron (positron) track finding to be 0.5% and the averaged uncertainties of positron and electron ID efficiency to be 0.03% and 0.10%, respectively.

B. K_L^0 Efficiency correction

We take the relative statistical uncertainty of the K_L^0 efficiency difference between data and MC as a function of momentum (as shown in Fig. 7 in the Appendix) as the uncertainty of the K_L^0 efficiency correction. Weighting these uncertainties by the K_L^0 momentum distribution in $D^+ \to K_L^0 e^+ \nu_e$, we obtain the uncertainties of the $K^0 \to K_L^0$ and $\bar{K}^0 \to K_L^0$ efficiency corrections to both be 1.2%.

C. Extra χ^2 cut for K_L^0 efficiency correction

As described in the Appendix, in the determination of the correction factor of the K_L^0 efficiency, we apply a χ^2 cut which brings an extra uncertainty. The uncertainty of the χ^2 cut is obtained by comparing the cut efficiency between data and MC using two control samples [$J/\psi \to K^*(892)^\pm K^\mp$ with $K^*(892)^\pm \to K_L^0 \pi^\pm$ and $J/\psi \to \phi K_L^0 K^\pm \pi^\mp$]. Weighting by the momentum distribution of the K_L^0 of signal events, the uncertainty of the extra χ^2 cut ($\chi^2 < 100$) is 0.8%.

D. Peaking backgrounds in DT

For Bkg II, from Eq. (7), the ratio of misreconstructed K_L^0 will not affect the measured branching fraction, since the numerator and the denominator share the common factor. The uncertainties of the peaking backgrounds of misreconstructed K_L^0 can be safely ignored. For Bkg III, Bkg IV, and Bkg V, we determine the change of the number of DT events by varying the branching fractions of peaking background channels by 1σ, and the uncertainty of peaking backgrounds in DT events is 1.6%.

E. $M_{\rm BC}$ fit

To evaluate the systematic uncertainty from the $M_{\rm BC}$ fit, we determine the changes of the DT yields divided by the ST yields when varying the standard deviation of the convoluted Gaussian function by $\pm 1\sigma$ deviation for each tag mode. We find that they are negligible.

The total systematic uncertainties of the branching fractions for $D^+ \to K_L^0 e^+ \nu_e$ and $D^- \to K_L^0 e^- \bar{\nu}_e$ are determined to be 2.3% and 2.3%, respectively, by adding all contributions in quadrature. In the determination of the *CP* asymmetry, the corresponding systematic uncertainties of branching fractions for $D^+ \to K_L^0 e^+ \nu_e$ and $D^- \to K_L^0 e^- \bar{\nu}_e$ are obtained in a similar fashion, except that the contribution of the extra χ^2 cut of the K_L^0 efficiency correction is not used since it cancels. The systematic uncertainties entering the *CP* asymmetry are found to be 2.1% and 2.1%, respectively.

V. HADRONIC FORM FACTOR

A. Method of extraction of form factor

The number of produced signal events for each tag mode from the whole q^2 range can be written as

$$n = 2N_{D^+D^-}\mathcal{B}_{\rm tag}\mathcal{B}_{\rm sig} = N_{\rm tag}\frac{\Gamma_{\rm sig}}{\Gamma_{D^+}}, \tag{9}$$

where $\Gamma_{\rm sig}$ is the partial decay width of $D^+ \to K_L^0 e^+ \nu_e$ while Γ_{D^+} is the total decay width of D^+. So we obtain

$$dn = \frac{N_{\rm tag}}{\Gamma_{D^+}} d\Gamma_{\rm sig} = N_{\rm tag}\tau_{D^+} d\Gamma_{\rm sig}, \tag{10}$$

where $\tau_{D^+} = 1/\Gamma_{D^+}$ is the D^+ lifetime and $d\Gamma_{\rm sig}$ is the differential decay width of the signal.

Substituting Eq. (10) into Eq. (1), Eq. (1) can be rewritten as

$$\frac{dn}{dq^2} = AN_{\rm tag}p^3|f_+(q^2)|^2, \tag{11}$$

where $A = \frac{1}{2}\frac{G_F^2|V_{cs}|^2}{24\pi^3}\tau_{D^+}$, and the number of observed semileptonic signal events as a function of q^2 is given by

$$\frac{dn_{\rm observed}}{dq^2} = AN_{\rm tag}[p^3(q'^2)|f_+(q'^2)|^2\epsilon(q'^2)] \otimes \sigma(q'^2, q^2), \tag{12}$$

where q'^2 refers to the true value and q^2 refers to the measured value, $p(q'^2)$ is the momentum of K_L^0 in the rest frame of the parent D, $\epsilon(q'^2)$ is the detection efficiency, and $\sigma(q'^2, q^2)$ is the detector resolution. To account for detector effects, we use the theoretical function convoluted with a Gaussian detector resolution to describe the observed signal curve.

B. Form-factor parametrizations

The goal of any particular parametrization $f_+(q^2)$ of the semileptonic form factors is to provide an accurate, and physically meaningful, expression of the strong dynamics in the decays. One possible way to achieve this goal is to express the form factors in terms of a dispersion relation. This approach of using dispersion relations and dispersive bounds in the description of form factors has been well established in the literature. In general, the dispersive representation is derived from the evaluation of the two point function [17,18] and can be written as

$$f_+(q^2) = \frac{f_+(0)}{(1-\alpha)}\frac{1}{1-\frac{q^2}{m_{\rm pole}^2}} + \frac{1}{\pi}\int_{(m_D+m_P)^2}^{\infty}\frac{{\rm Im}f_+(t)}{t-q^2-i\epsilon}dt, \tag{13}$$

where m_D and m_P are the masses of the D meson and pseudoscalar meson, respectively, while $m_{\rm pole}$ is the mass of the lowest-lying $c\bar{q}$ vector meson, with $c \to q$ the quark transition of the semileptonic decay. For the charm semileptonic decays, we have $m_{\rm pole} = m_{D_s^*}$ for $D \to Ke\nu_e$ decays. The parameter α expresses the size of the vector meson pole contribution to $f_+(0)$. It is common to write the contribution from the continuum integral as a sum of effective poles

$$f_+(q^2) = \frac{f_+(0)}{(1-\alpha)}\frac{1}{1-\frac{q^2}{m_{\rm pole}^2}} + \sum_{k=1}^{N}\frac{\rho_k}{1-\frac{1}{\gamma_k}\frac{q^2}{m_{\rm pole}^2}}, \tag{14}$$

where ρ_k and γ_k are expansion parameters.

The simplest parametrization, known as the simple pole model, assumes that the sum in Eq. (14) is dominated by a single pole,

$$f_+(q^2) = \frac{f_+(0)}{1-\frac{q^2}{m_{\rm pole}^2}}, \tag{15}$$

where the value of $m_{\rm pole}$ is predicted to be $m_{D_s^*}$. In experiments, $m_{\rm pole}$ is left as a free fit parameter to improve the fit quality.

Another parametrization is known as the modified pole model, or Becirevic-Kaidelov parametrization [14]. The idea is to add the first term in the effective pole expansion, while making simplifications such that the form factor can be determined with only two parameters: the intercept $f_+(0)$ and an additional shape parameter α. The simplified one-term expansion is usually written in the form

$$f_+(q^2) = \frac{f_+(0)}{(1-\frac{q^2}{m_{\rm pole}^2})(1-\alpha\frac{q^2}{m_{\rm pole}^2})}. \tag{16}$$

A third parametrization is known as the series expansion [19]. Exploiting the analytic properties of $f_+(q^2)$, a transformation of variables is made that maps the cut in the q^2 plane onto a unit circle $|z| < 1$, where

$$z(q^2, t_0) = \frac{\sqrt{t_+ - q^2} - \sqrt{t_+ - t_0}}{\sqrt{t_+ - q^2} + \sqrt{t_+ - t_0}}, \tag{17}$$

$t_\pm = (m_D \pm m_P)^2$, and t_0 is any real number less than t_+. This transformation amounts to expanding the form factor about $q^2 = t_0$, with the expanded form factor given by

$$f_+(q^2) = \frac{1}{P(q^2)\phi(q^2, t_0)}\sum_{k=0}^{\infty}a_k(t_0)[z(q^2, t_0)]^k, \tag{18}$$

where a_k are real coefficients, $P(q^2) = z(q^2, M_{D_s^*}^2)$ for kaon final states, $P(q^2) = 1$ for pion final states, and $\phi(q^2, t_0)$ is any function that is analytic outside a cut in the complex q^2 plane that lies along the x axis from t_+ to ∞. This expansion has improved convergence properties over Eq. (14) due to the smallness of z, for example, taking the traditional choice of $t_0 = t_+(1-(1-t_-/t_+)^{1/2})$, which minimizes the maximum value of $z(q^2, t_0)$. Further, taking the standard choice of ϕ,

$$\phi(q^2, t_0) = \sqrt{\frac{\pi m_c^2}{3}}\left(\frac{z(q^2,0)}{-q^2}\right)^{5/2}\left(\frac{z(q^2,t_0)}{t_0-q^2}\right)^{-1/2} \times \left(\frac{z(q^2,t_-)}{t_- - q^2}\right)^{-3/4}\frac{t_+ - q^2}{(t_+ - t_0)^{1/4}}, \tag{19}$$

where m_c is the mass of charm quark and it can be shown that the sum over all k of a_k^2 is of order unity.

In practical use of the series expansion form factor, one often takes $k=1$ and $k=2$ in Eq. (18), which gives following two forms of the form factor.

(i) 2 parameter series expansion of the form factor is given by

$$f_+(q^2)=\frac{1}{P(q^2)\phi(q^2,t_0)}a_0(t_0)(1+r_1(t_0)[z(q^2,t_0)]). \tag{20}$$

It can be rewritten as

$$f_+(q^2)=\frac{1}{P(q^2)\phi(q^2,t_0)}\frac{f_+(0)P(0)\phi(0,t_0)}{1+r_1(t_0)z(0,t_0)} \times(1+r_1(t_0)[z(q^2,t_0)]), \tag{21}$$

where $r_1=a_1/a_0$.

(ii) 3 parameter series expansion of the form factor is given by

$$f_+(q^2)=\frac{1}{P(q^2)\phi(q^2,t_0)}a_0(t_0) \times(1+r_1(t_0)[z(q^2,t_0)] +r_2(t_0)[z(q^2,t_0)]^2). \tag{22}$$

It can be rewritten as

$$f_+(q^2)=\frac{1}{P(q^2)\phi(q^2,t_0)} \times\frac{f_+(0)P(0)\phi(0,t_0)}{1+r_1(t_0)z(0,t_0)+r_2(t_0)z^2(0,t_0)} \times(1+r_1(t_0)[z(q^2,t_0)] +r_2(t_0)[z(q^2,t_0)]^2), \tag{23}$$

where $r_1=a_1/a_0$, $r_2=a_2/a_0$.

C. Determination of $f_+^K(0)|V_{cs}|$

We perform simultaneous fits to the distributions of observed DT candidates as a function of q^2 for the six ST modes to determine $f_+^K(0)|V_{cs}|$. In the fits, we treat D^+ and D^- DT candidates together. The detection efficiency $\epsilon(q'^2)$ and detector resolution $\sigma(q'^2,q^2)$ are obtained from the K_L^0 efficiency corrected signal MC simulations. For each ST mode, $\epsilon(q'^2)$ is described by a fourth-order polynomial; the $(q^2-q'^2)$ distribution is described by a Gaussian function. As an example, Fig. 5 shows the fits to $\epsilon(q'^2)$ for signal events tagged by $D^\pm\to K^\mp\pi^\pm\pi^\pm$.

Simultaneous fits are made with one or two common parameters related to the form-factor shape to the data for the simple pole model ($m_{\rm pole}$), the modified pole model (α), two-parameter series expansion (r_1) and three-parameter series expansion (r_1, r_2). As an example, Fig. 6 shows the simultaneous fit results using the two-parameter series expansion model. The signal Probability Density Function is constructed in the form of Eq. (12). For the background shape, as mentioned in Sec. III C, the shape and the number of Bkg I events are fixed according to the side-band region of the $M_{\rm BC}$ distribution ($1.83<M_{\rm BC}<1.85$ GeV/c^2) from data; for Bkgs from II to V, the shape is determined from the K_L^0 efficiency corrected generic MC samples. We also fix the relative proportion of $N_{\rm sig}$, $N_{\rm Bkg\,II}$, and $N_{\rm Bkg\,III}+N_{\rm Bkg\,IV}$ events, to the result from the K_L^0 efficiency corrected generic MC. Here, $N_{\rm sig}$, $N_{\rm Bkg\,II}$, $N_{\rm Bkg\,III}$, and $N_{\rm Bkg\,IV}$ represent the numbers of the signal, Bkg II, Bkg III, and Bkg IV events, respectively.

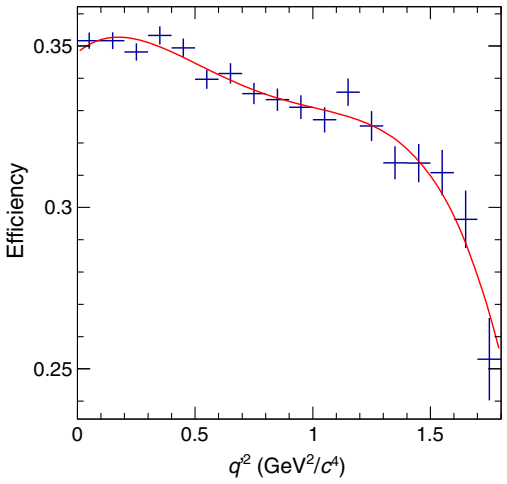

FIG. 5 (color online). Detection efficiency $\epsilon(q'^2)$ for signal events tagged by $D^\pm\to K^\mp\pi^\pm\pi^\pm$. The dots with error bars are the corrected signal MC efficiencies, and the curve is the fit result.

The product $f_+^K(0)|V_{cs}|$ is obtained from

$$f_+^K(0)|V_{cs}|=\sqrt{\frac{48\pi^3}{G_F^2}\frac{N_{\rm sig}}{N_{\rm tag}\tau_{D^+}I}}, \tag{24}$$

where $I=\int[p^3(q'^2)|f_+(q'^2)|^2\epsilon(q'^2)]\otimes\sigma(q'^2,q^2)dq^2$.

Since the q^2 distribution of the signal events is smooth, the form-factor fit is insensitive to the detector resolution. For each tag mode, we use the full width at half maximum (FWHM) of the $(q^2-q'^2)$ distribution to estimate $\sigma(q'^2,q^2)$ and obtain FWHM $=0.0360$ GeV$^2/c^4$ and the corresponding resolution $\sigma=\text{FWHM}/2\sqrt{2\ln 2}=0.0153$ GeV$^2/c^4$. The distributions of DT candidates as a function of q^2 are fit again by different models with the detector resolution $\sigma=0.0153$ GeV$^2/c^4$. Compared to the previous results, the form-factor parameters and the signal yields are almost unchanged. So the uncertainty of the detector resolution can be ignored in the form-factor fit.

Systematic uncertainties of the form-factor parameters are more sensitive to the distribution of backgrounds in this analysis. We use a different side-band region of the $M_{\rm BC}$

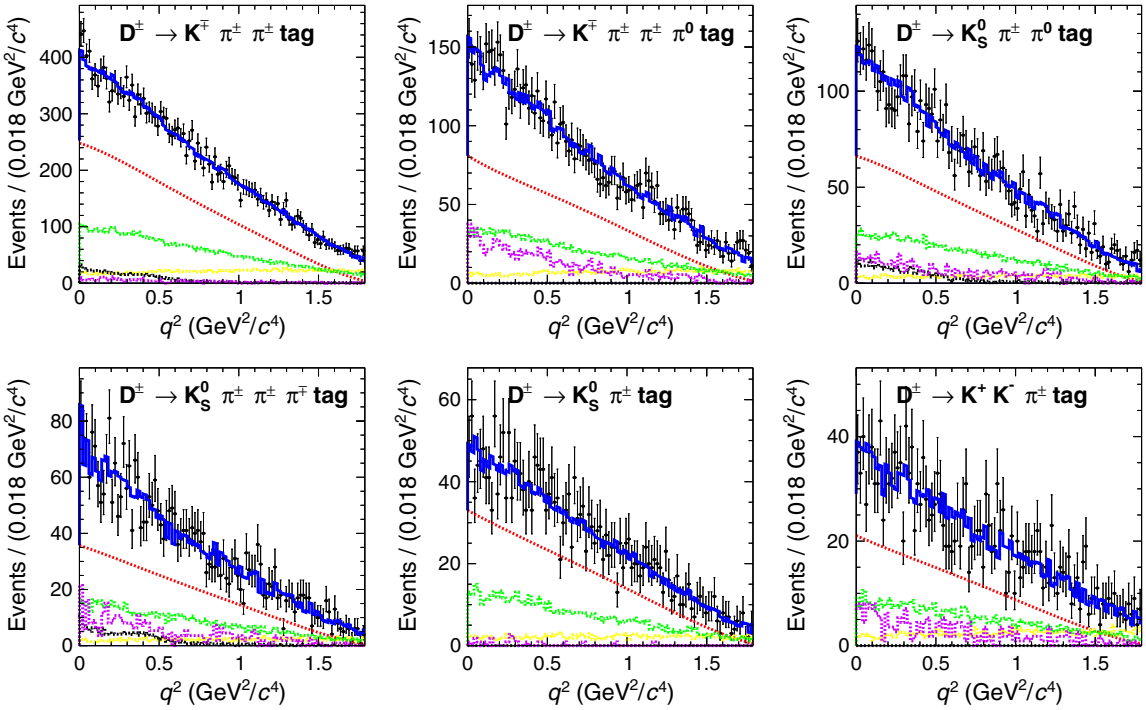

FIG. 6 (color online). Simultaneous fit to the numbers of DT candidates as a function of q^2 with the two-parameter series expansion parametrization. The points are data, and the curves are the fit to data. In each plot, the violet, yellow, green, and black curves refer to Bkg I, Bkg II, Bkg III + Bkg IV, and Bkg V, respectively. The red dashed curve shows the contribution of signal, and the blue solid curve shows the sum of the background and signal.

distribution ($1.835 < M_{\rm BC} < 1.855$ GeV/c^2) and ISGW2 model to simulate the main possible semileptonic backgrounds. We simultaneously fit the distributions of observed DT candidates as a function q^2 again. The differences between the form-factor parameters obtained from the two determinations are taken as the systematic uncertainties of the form-factor parameters.

Systematic uncertainties associated with the product $f_+^K(0)|V_{cs}|$ are one-half of the systematic uncertainties in the branching fraction measurements, presented in Sec. IV, combined in quadrature with the uncertainties associated with the D^+ lifetime (0.67%) [13] and the integration I, which are obtained by varying the form-factor parameters by $\pm 1\sigma$. The systematic uncertainties of $f_+^K(0)|V_{cs}|$ are

TABLE IV. Comparison of results of $f_+^K(0)|V_{cs}|$ and shape parameters ($m_{\rm pole}$, α, r_1, and r_2) to previous corresponding results determined by $D^+ \to K_S^0 e^+ \nu_e$ from CLEO-c [16]. The first uncertainties are statistical, and the second are systematic.

Single pole model		
Decay mode	$f_+^K(0)\|V_{cs}\|$	$m_{\rm pole}$(GeV/c^2)
$D^+ \to K_L^0 e^+ \nu_e$	$0.729 \pm 0.006 \pm 0.010$	$1.953 \pm 0.044 \pm 0.036$
$D^+ \to K_S^0 e^+ \nu_e$	$0.720 \pm 0.006 \pm 0.009$	$1.95 \pm 0.03 \pm 0.01$
Modified pole model		
Decay mode	$f_+^K(0)\|V_{cs}\|$	α
$D^+ \to K_L^0 e^+ \nu_e$	$0.727 \pm 0.006 \pm 0.011$	$0.239 \pm 0.077 \pm 0.065$
$D^+ \to K_S^0 e^+ \nu_e$	$0.715 \pm 0.007 \pm 0.009$	$0.28 \pm 0.06 \pm 0.02$
Two-parameter series expansion		
Decay mode	$f_+^K(0)\|V_{cs}\|$	r_1
$D^+ \to K_L^0 e^+ \nu_e$	$0.728 \pm 0.006 \pm 0.011$	$-1.91 \pm 0.33 \pm 0.28$
$D^+ \to K_S^0 e^+ \nu_e$	$0.716 \pm 0.007 \pm 0.009$	$-2.10 \pm 0.25 \pm 0.08$
Three-parameter series expansion		
Decay mode	$f_+^K(0)\|V_{cs}\|$	r_1 $\quad$ r_2
$D^+ \to K_L^0 e^+ \nu_e$	$0.737 \pm 0.006 \pm 0.009$	$-2.23 \pm 0.42 \pm 0.53$ $\quad$ $11.3 \pm 8.5 \pm 8.7$
$D^+ \to K_S^0 e^+ \nu_e$	$0.707 \pm 0.010 \pm 0.009$	$-1.66 \pm 0.44 \pm 0.10$ $\quad$ $-14 \pm 11 \pm 1$

obtained for the simple pole model, modified pole model, two-parameter series expansion, and three-parameter series expansion to be 1.4%, 1.5%, 1.5%, and 1.2%, respectively.

The fit results are given in Table IV. As a comparison, Table IV also lists the corresponding form-factor results determined for $D^+ \to K_S^0 e^+ \nu_e$ from CLEO-*c* [16]. Our results are consistent with those from CLEO-*c* within uncertainties except for three-parameter series expansion model due to heavy backgrounds in this analysis. In general, as long as the normalization and at least one shape parameter are allowed to float, all models describe the data well. We choose the two-parameter series fit to determine $f_+^K(0)$ and $|V_{cs}|$.

The BESIII experiment has recently reported the most precise value of $f_+^K(0)|V_{cs}|$ using the two-parameter series expansion for $D^0 \to K^- e^+ \nu_e$ [20]. It is in agreement with the results reported here.

D. Determination of $f_+^K(0)$ and $|V_{cs}|$

Using the $f_+^K(0)|V_{cs}|$ value from the two-parameter series expansion fit and $|V_{cs}| = 0.97343 \pm 0.00015$ from PDG fits assuming CKM unitarity [13] or $f_+^K(0) = 0.747 \pm 0.019$ from the unquenched LQCD calculation [21] as input, we obtain

$$f_+^K(0) = 0.748 \pm 0.007 \pm 0.012 \tag{25}$$

and

$$|V_{cs}| = 0.975 \pm 0.008 \pm 0.015 \pm 0.025, \tag{26}$$

where the uncertainties are statistical, systematic, and external [in Eq. (26)]. For Eq. (25), the external error is negligible (0.0002) compared to our measurement. The measured $f_+^K(0)$ is consistent with the one measured with $D^+ \to K_S^0 e^+ \nu_e$ at CLEO-*c* [16]; it is also in good agreement with LQCD predictions, although the currently available LQCD results have relatively large uncertainties. The measured $|V_{cs}|$ is in agreement with that reported by the PDG.

VI. SUMMARY

In this paper, we present the first measurement of the absolute branching fraction $\mathcal{B}(D^+ \to K_L^0 e^+ \nu_e) = (4.481 \pm 0.027(\text{stat}) \pm 0.103(\text{sys}))\%$, which is in excellent agreement with $\mathcal{B}(D^+ \to K_S^0 e^+ \nu_e)$ measured by CLEO-*c* [16]. The *CP* asymmetry $A_{CP}^{D^+ \to K_L^0 e^+ \nu_e} = (-0.59 \pm 0.60(\text{stat}) \pm 1.48(\text{sys}))\%$, which agrees with the theoretical prediction on *CP* violation in the K^0 system within the statistical error, is also determined. By fitting the distributions of the observed DT events as a function of q^2, $f_+^K(0)|V_{cs}|$ and the corresponding parameters for three different theoretical form-factor models are determined. Taking $f_K^+(0)|V_{cs}|$ from the two-parameter series expansion parametrization, $f_K^+(0)|V_{cs}| = 0.728 \pm 0.006(\text{stat}) \pm 0.011(\text{sys})$, and using $|V_{cs}|$ from the SM constraint fit, we find $f_+^K(0) = 0.748 \pm 0.007(\text{stat}) \pm 0.012(\text{sys})$. By using an unquenched LQCD prediction for $f_+^K(0)$, $|V_{cs}| = 0.975 \pm 0.008(\text{stat}) \pm 0.015(\text{sys}) \pm 0.025(\text{LQCD})$.

ACKNOWLEDGMENTS

The BESIII Collaboration thanks the staff of BEPCII and the IHEP computing center for their strong support. This work is supported in part by National Key Basic Research Program of China under Contract No. 2015CB856700; National Natural Science Foundation of China (NSFC) under Contracts No. 11125525, No. 11235011, No. 11322544, No. 11335008, and No. 11425524; the Chinese Academy of Sciences (CAS) Large-Scale Scientific Facility Program; the CAS Center for Excellence in Particle Physics; the Collaborative Innovation Center for Particles and Interactions; Joint Large-Scale Scientific Facility Funds of the NSFC and CAS under Contracts No. 11179007, No. U1232201, and No. U1332201; CAS under Contracts No. KJCX2-YW-N29 and No. KJCX2-YW-N45; 100 Talents Program of CAS; National 1000 Talents Program of China; INPAC and Shanghai Key Laboratory for Particle Physics and Cosmology; German Research Foundation DFG under Contract No. Collaborative Research Center CRC-1044; Istituto Nazionale di Fisica Nucleare, Italy; Ministry of Development of Turkey under Contract No. DPT2006K-120470; Russian Foundation for Basic Research under Contract No. 14-07-91152; The Swedish Research Council; US Department of Energy under Contracts No. DE-FG02-04ER41291, No. DE-FG02-05ER41374, No. DE-SC0012069, and No. DESC0010118; US National Science Foundation; University of Groningen and the Helmholtzzentrum fuer Schwerionenforschung GmbH, Darmstadt; and WCU Program of National Research Foundation of Korea under Contract No. R32-2008-000-10155-0. This work is also supported by the NSFC under Contracts No. 11275209 and No. 11475107.

APPENDIX: SYSTEMATIC UNCERTAINTY IN K_L^0 RECONSTRUCTION EFFICIENCY

To determine the systematic uncertainty in the K_L^0 reconstruction efficiency, we measure the K_L^0 efficiency in data and MC using a partial reconstruction technique. We then determine the efficiency difference between data and MC, $\epsilon_{\text{data}}/\epsilon_{\text{MC}} - 1$, of the K_L^0 reconstruction efficiency, where ϵ_{MC} is the efficiency for MC and ϵ_{data} is the efficiency for data.

Based on 1.3 B J/ψ events collected by the BESIII detector in the years 2009 and 2012, we use two control samples to measure K_L^0 reconstruction efficiency. One sample is $J/\psi \to K^*(892)^\pm K^\mp$ with $K^*(892)^\pm \to K_L^0 \pi^\pm$,

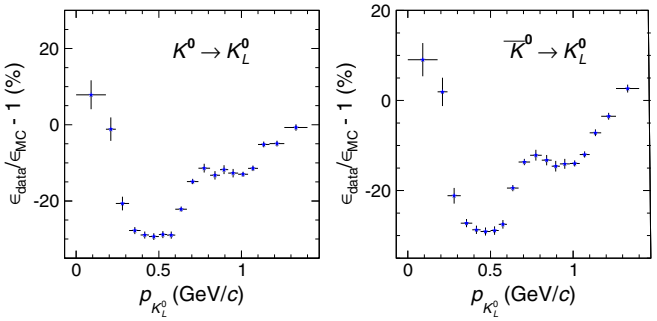

FIG. 7 (color online). Distributions of K^0_L reconstruction efficiency differences between data and MC for the processes of $K^0 \to K^0_L$ and $\bar{K}^0 \to K^0_L$.

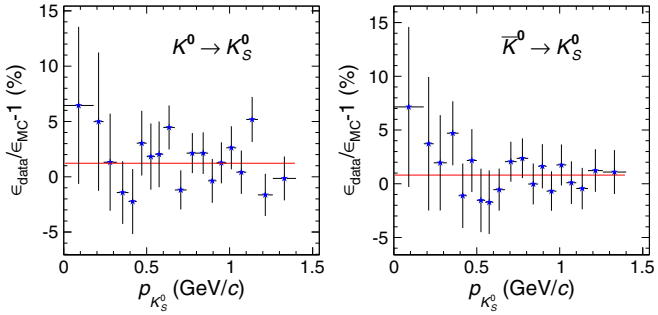

FIG. 8 (color online). Distributions of K^0_S reconstruction efficiency differences between the data and MC for the processes of $K^0 \to K^0_S$ and $\bar{K}^0 \to K^0_S$. The red line is the fit to the points in the form of a zero-order polynomial.

and the other is $J/\psi \to \phi K^0_L K^\pm \pi^\mp$. We reconstruct all the particles in the event except the K^0_L of which the efficiency we wish to measure. The number of $K^0(\bar{K}^0)$ is denoted by N_1. Then, by applying K^0_L selection requirements mentioned in Sec. III B, we obtain the number of $K^0(\bar{K}^0)$ denoted by N_2. Here, in order to select K^0_L control samples with a low level of backgrounds, we perform the kinematic fit to select the K^0_L candidate with the minimal χ^2 and require $\chi^2 < 100$.

The $K^0(\bar{K}^0)$ reconstruction efficiency is calculated by $\epsilon = N_2/N_1$. For data, N_1, N_2 are determined by fitting the missing mass squared distribution of K^0_L. Each fit includes a signal line shape function which is determined from MC samples smeared with a Gaussian resolution, and the background shape is determined from MC samples as well. With respect to MC samples, N_1, N_2 are obtained from MC truth directly. The fits are performed in separate momentum bins. In each fit, $N_1(N_2)$ consists of the number of K^0_L and K^0_S. The ratio of K^0_L to K^0_S is estimated from MC simulations. Due to the effect of the difference in nuclear interactions of K^0 and $\bar{K}^0$ mesons, we consider $K^0 \to K^0_L$ and $\bar{K}^0 \to K^0_L$ separately. We use the charge of the kaon to tag K^0 or $\bar{K}^0$ in the control sample, which means if we find a K^+ in the process, the corresponding K^0_L must be derived from $\bar{K}^0$.

Figure 7 shows the distributions of K^0_L reconstruction efficiency differences between data and MC in 19 momentum bins for the processes of $K^0 \to K^0_L$ and $\bar{K}^0 \to K^0_L$.

The probability of an inelastic interaction of a neutral kaon in the detector depends on the strangeness of the kaon at any point along its path, which is due to oscillations in kaon strangeness and different nuclear cross sections for K^0 and $\bar{K}^0$. Hence, the total efficiency to observe a final state $K^0_L(K^0_S)$ differs from that expected for either K^0 or $\bar{K}^0$. This effect is related to the coherent regeneration of neutral kaons [22]. However, the detector-simulation program GEANT4 does not take into account this effect. The time-dependent $K^0 - \bar{K}^0$ oscillations are thereby ignored in GEANT4. Considering the massive detector materials in the outer of the MDC, the TOF counter and the EMC, it results in an obvious discrepancy (>10%) of the K^0_L shower-finding efficiency in the EMC between the data and MC. On the other hand, we take the same method to study the K^0_S reconstruction efficiency difference between the data and MC for the processes of $K^0 \to K^0_S$ and $\bar{K}^0 \to K^0_S$ by a 224 M J/ψ control sample, as shown in Fig. 8. We find that the K^0_S reconstruction efficiency of the data is a little higher than that of MC, which gives another hint of the absence of the coherent regeneration of neutral kaons by GEANT4.

[1] M. Kobayashi and T. Maskawa, Prog. Theor. Phys. **49**, 652 (1973).
[2] N. Cabibbo, Phys. Rev. Lett. **10**, 531 (1963).
[3] F. Buccella, M. Lusignoli, G. Miele, A. Pugliese, and P. Santorelli, Phys. Rev. D **51**, 3478 (1995); Y. Grossman, A. L. Kagan, and Y. Nir, Phys. Rev. D **75**, 036008 (2007).
[4] Z. Z. Xing, Phys. Lett. B **353**, 313 (1995); **363**, 266 (1995).
[5] M. Ablikim *et al.* (BESIII Collaboration), Chin. Phys. C **37**, 123001 (2013).
[6] M. Ablikim *et al.* (BESIII Collaboration), Nucl. Instrum. Methods Phys. Res., Sect. A **614**, 345 (2010).
[7] C. Zhang, Sci. China, Ser. G: Phys., Mech. Astron., **53**, 2084 (2010).
[8] S. Agostinelli*et al.* (GENAT4 Collaboration), Nucl. Instrum. Methods Phys. Res., Sect. A **506**, 250 (2003).

[9] S. Jadach, B. F. L. Ward, and Z. Was, Phys. Rev. D **63**, 113009 (2001).
[10] E. Barberio and Z. Was, Comput. Phys. Commun. **79**, 291 (1994).
[11] D. J. Lange, Nucl. Instrum. Methods Phys. Res., Sect. A **462**, 152 (2001).
[12] R. G. Ping, Chin. Phys. C **32**, 599 (2008).
[13] K. A. Olive *et al.*, Chin. Phys. C **38**, 090001 (2014).
[14] D. Becirevic and A. B. Kaidalov, Phys. Lett. B **478**, 417 (2000).
[15] H. Albrecht *et al.* (ARGUS Collaboration), Phys. Lett. B **241**, 278 (1990).
[16] D. Besson *et al.* (CLEO Collaboration), Phys. Rev. D **80**, 032005 (2009).
[17] C. Glenn Boyd, B. Grinstein, and R. F. Lebed, Phys. Rev. Lett. **74**, 4603 (1995).
[18] C. Glenn Boyd and M. J. Savage, Phys. Rev. D **56**, 303 (1997).
[19] T. Becher and R. J. Hill, Phys. Lett. B **633**, 61 (2006).
[20] M. Ablikim *et al.* (BESIII Collaboration), Phys. Rev. D **92**, 072012(2015).
[21] H. Na, C. T. H. Davies, E. Follana, G. P. Lepage, and J. Shigemitsu (HPQCD Collaboration), Phys. Rev. D **82**, 114506 (2010).
[22] A. Pais and O. Piccioni, Phys. Rev. **100**, 1487 (1955).